Pharmaceutical Research, Vol. 22, No. 5, May 2005 (© 2005)
DOI: 10.1007/s11095-005-2585-8

Research Paper

P-Glycoprotein Induction and Tumor Cell-Kill Dynamics in Response to Differential Doxorubicin Dosing Strategies: A Theoretical Pharmacodynamic Model

Kenneth T. Luu[1] and James A. Uchizono[1,2]

Received December 10, 2004; accepted January 28, 2005

Purpose. The objectives of this work were 1) to develop a theoretical pharmacodynamic model that captures dynamic changes resulting from drug/therapy mediated P-glycoprotein (P-gp) induction and 2) to compare the pharmacodynamic outcomes of several doxorubicin (DOX) dosing schemes through simulations.
Methods. We developed a theoretical model that included a pharmacokinetic (PK) model for intracellular DOX-mediated P-gp induction and a pharmacodynamic (PD) model using a threshold trigger function for tumor cell-kill. In this model, both the level of P-gp induction and rate of tumor cell death were modulated by intracellular DOX concentration. Most model parameters were obtained from literature sources, and a few were either fixed or reasonably estimated.
Results. Comparative dosing simulations showed that a 10-week constant infusion in which a tumor cell population was continuously exposed to the drug did not produce the best PD profile. On the other hand, dosing schemes where the cell population was initially challenged with a high dose, followed by intermittent dosing, generated the best PD profile. The favorable outcome of the latter dosing schemes was correlated with the lowest expression of P-gp in terms of area under the curve (AUC) during treatment period.
Conclusions. The simulations led us to conclude that drug resistance, particularly resistance caused by P-gp overexpression, induced during chemotherapy may, in part, be circumvented by designing optimal dosing strategies that minimize P-gp induction.

KEY WORDS: drug resistance; doxorubicin; p-glycoprotein; pharmacodynamic; optimal dosing.

INTRODUCTION

A major mechanism of drug resistance in chemotherapy is the overexpression of multidrug resistance (MDR) genes encoding P-glycoprotein (P-gp) and multidrug resistance–associated protein (MRP). Both P-gp and MRP are transmembrane proteins, which are energy-dependent efflux pumps capable of effectively reducing intracellular accumulation of structurally unrelated cytotoxic agents (1). P-glycoprotein, in particular, has been shown to lower intracellular accumulation of agents such as anthracyclines, antineoplastic agents, vinca alkaloids, and taxol (2). Several *in vitro* studies have demonstrated that anticancer agents such as doxorubicin (3) and cisplatin (4) cause increases in the protein expression level of P-gp during treatment periods. Especially interesting in these studies is the time course of induction, which shows that the overexpressed P-gp level returns to its basal level when the treatment is discontinued. These lines of evidence would lead one to speculate on the time course of P-gp expression level in tumor cells during chronic chemotherapy. We postulated that, because P-gp induction during therapy depends on the size and previous exposure history of each dose, the time course of P-gp induction would be affected by dosing schedule. Furthermore, P-gp induction is a clinically recognized problem, reducing therapeutic efficacy. Therefore, there remains a need for pharmacokinetic/pharmacodynamic (PK/PD) tumor models that incorporate P-gp induction dynamics.

Doxorubicin (DOX) is a known substrate of P-glycoprotein and is a widely used, first-line agent, anthracycline antibiotic for a variety of solid and hematological tumors. Several mechanisms of cytotoxicity have been suggested for doxorubicin including induction of apoptotic death signals (5) and DNA intercalation as well as inhibition of topoisomerase II religation activity during DNA synthesis (6). The mechanism by which DOX induces apoptosis has been controversial and may vary depending on cell type. In S-type neuroblastoma cells, for example, earlier works have shown that DOX causes increased expression of CD95/Fas, FasL mRNA and subsequent activation of caspase-8 (7). More recently, activation of caspase-9, instead of caspase-8, was found to be important in eliciting death signals in these cell types (5). Notwithstanding the facts, these proposed mechanisms of cell-kill point to the nucleus as the main intracellular site of action where sequestration of DOX is re-

[1] Department of Pharmaceutics and Medicinal Chemistry, University of the Pacific, Stockton, California, USA 95211.
[2] To whom correspondence should be addressed. (e-mail: juchizono@pacific.edu)

quired to trigger cell death. Thus, PD models of the tumor cell-kill kinetics of DOX should include a nuclear compartment.

In this paper, we present a theoretical pharmacodynamic model that describes the changes in tumor cell-kill kinetics secondary to doxorubicin (DOX)-modulation of P-gp levels. By extending the work of Dordal *et al.* (8) and Jackson (9) to include P-gp induction dynamics, we are able to use many parameters found in their work. Key aspects of this model are 1) nuclear accumulation of DOX greater than a threshold amount is required for cell death, and 2) P-gp induction dynamics are linked to dosing size and prior exposure history through the kinetics of the intracellular (ICF) compartment. We hypothesized that each DOX dosing strategy, all constrained to a total dose of 500 mg/10 weeks, would produce a unique P-pg induction profile, with each profile producing a different PD outcome or tumor cell-kill profile.

MATERIALS AND METHODS

Pharmacokinetics

The overall system is schematically represented in Fig. 1. The PK model was not based on actual pharmacokinetic parameters for DOX but on a three-compartment cellular transport model previously published by Dordal *et al.* (8). Differently in this work, we added two additional exit rate constants (k_{10} and k_{30}) in order to extend the original cellular model to a physiologic one that can account for drug elimination (Fig. 2a). For simplicity, it was assumed that DOX can be dosed directly to the extracellular fluid (ECF) compartment. In keeping with the original work of Dordal *et al.,* the third compartment, "nucleus" (NUC), was made "nonexchangeable" and, therefore, k_{32} was not implemented. This assumption was supported by their model fitting of fluorescent data obtained from transport studies on S-type neuroblastoma cells (8). In order to use the parameters estimated from experimental data in Jackson (9) and Dordal (8), we chose to minimally alter their models, which led to keeping the nonexchangeable NUC compartment.

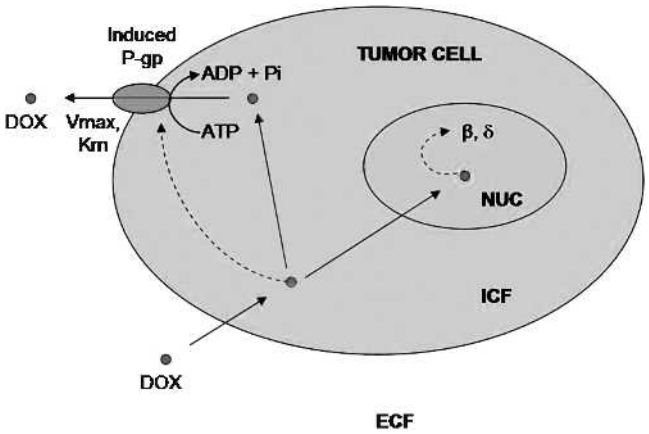

Fig. 1. Schematic representation of the kinetic phenomenon being modeled. From the ECF, DOX is transported into and accumulated in the ICF of the tumor cell where it causes P-gp to be induced to a higher level. Increases in the amount of P-gp leads to increases in V_{max}. Tumor cell-kill depends on a trigger function with a threshold δ and the kill rate constant, β. The dotted line pointing from DOX to the P-gp transporter indicates an *indirect* DOX modulation of P-gp, and the dotted line pointing to β indicates DOX triggered cell kill.

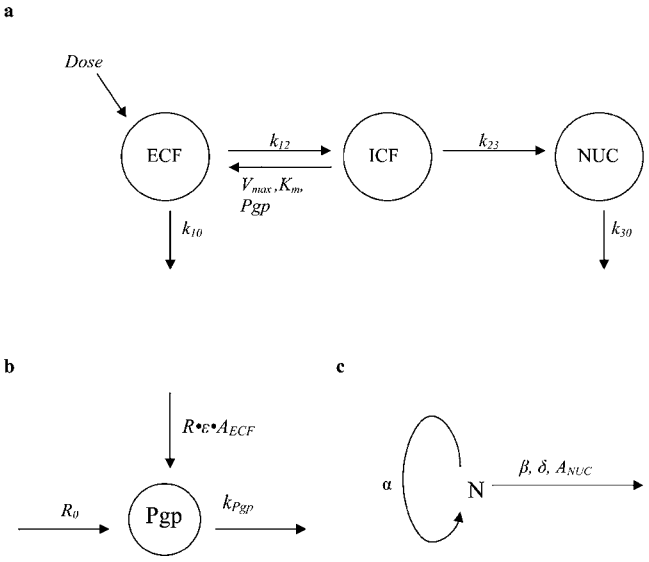

Fig. 2. (a) The 3-compartment PK model was developed based on a previously published 3-compartment kinetic model of cellular transport (see text). ECF, extracellular compartment; ICF, intracellular compartment, which mediates Pgp induction; NUC, a "nonexchangeable" compartment, possibly nucleus, where triggered cell death is mediated. (b) The time course of Pgp was characterized by a turnover model with basal input and output rate constants. In addition, intracellular (ICF) levels of DOX modulate Pgp induction (see text and equations). (c) Tumor cell-kill kinetics was characterized by a cell cycle nonspecific killing with a trigger function (see text and equations).

Shown in Fig. 2b is the linked model for P-gp induction. The kinetics of Pgp induction was characterized by an induction term *R,* which can be modulated by the amount of drug (A_{ICF}) in the ICF compartment, in addition to the basal zero-order input and first-order exit rate constants R_0 and k_{Pgp}, respectively. ε is a conversion factor (see "Differential Equations," below).

Pharmacodynamics

The PD model was characterized by a simple, cell-cycle nonspecific model (10) that incorporated a trigger function for cell kill (Fig. 2c). In this model, the number of surviving tumor cells (N) is governed by the intrinsic growth rate constant, α, and the maximal cell-kill rate constant, β. The kill kinetics was linked to the amount of accumulated drug in the NUC compartment (A_{NUC}) and a trigger threshold, δ, required for initiating cell kill. This trigger function was modeled after Jackson's (9) previous work.

Differential Equations

The mathematical expressions are presented in Eqs. (1)–(5). Equations (1)–(3) represent mass-balance relationships for a three-compartment model (Fig. 2a). V_{max} is the limiting factor, which describes the maximum efflux transport of drug from the ICF compartment to the ECF compartment. To avoid identifiability and scaling issues, the relationship between P-gp and V_{max} was simplified by using a single parameter, λ. This term is simply a scaling conversion factor that

relates the actual *Pgp* level to V_{max}. For the same reason, ε, a term that scales A_{ICF} to the P-gp induction constant *R*, was also used in Eq. (4). In this equation, *Pgp* represents the P-gp protein level (hypothetical unit) with intrinsic production term, R_0, and turnover term, k_{Pgp}. The presence of drug in the ICF compartment modulates the P-gp induction term *R,* which is zero when no drug is present in this compartment.

$$\frac{dA_{ECF}}{dt} = dose + \frac{V_{max} \cdot \lambda \cdot Pgp \cdot A_{ICF}}{k_m + A_{ICF}} - (k_{12} + k_{10})A_{ECF} \quad (1)$$

$$\frac{dA_{ICF}}{dt} = k_{12} \cdot A_{ECF} - \left(\frac{V_{max} \cdot \lambda \cdot Pgp}{k_m + A_{ICF}} - k_{23}\right)A_{ICF} \quad (2)$$

$$\frac{dA_{NUC}}{dt} = k_{23} \cdot A_{ICF} - k_{30} \cdot A_{NUC} \quad (3)$$

$$\frac{dPgp}{dt} = R_0 + R \cdot \varepsilon \cdot A_{ICF} - k_{Pgp} \cdot Pgp \quad (4)$$

$$\frac{dN}{dt} = \left[\alpha - \frac{\beta \cdot A_{NUC}''}{(\delta + A_{NUC})^n}\right]N \quad (5)$$

Equation (5) [modified from Jackson (9)] depicts changes to a given cancer cell population *N*. The term α is the intrinsic growth rate constant of the cell population, δ and *n* define a switch function that triggers cell death, and β determines the maximal rate of drug-induced cell kill. For simplicity, the terms λ in Eq. (1) and *n* in Eq. (5) were fixed to unity. Table I lists the parameter values and their references.

RESULTS

The simulations for different dosing schemes returned expected concentration profiles for the pharmacokinetic component of our model (results not shown). DOX reached steady state rapidly in the ICF and slightly slower in the NUC as expected. Shown in Fig. 3 is the pharmacodynamic result for all five different dosing schemes, shown in Table II. As shown in this figure, a 500 mg dosing of any schedule (dash lines) over 10 weeks significantly reduced tumor growth as compared to no treatment (solid line). For quantitative comparison, AUC (area under the curve) was calculated for these curves (Table III). Based on AUC comparison, a 50-mg IV bolus once a week (IVB QW) treatment over 10 weeks (*S-II*) shows significantly better tumor growth management compared to a constant infusion (*S-I*). Among the four dosing schemes, *S-III* and *S-IV* produced nearly identical AUC results with *S-III* having only a slightly smaller growth curve AUC.

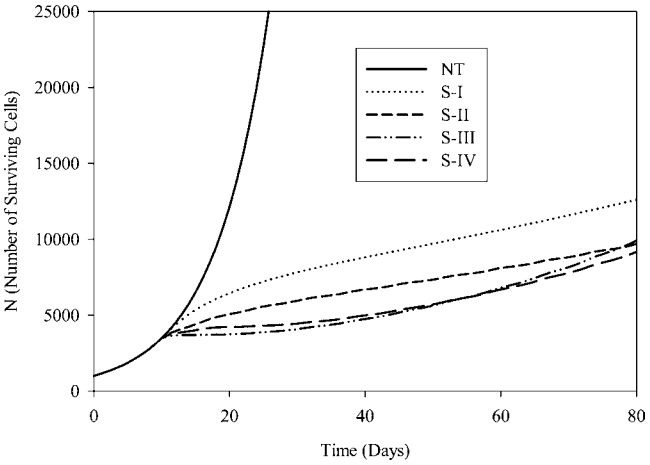

Fig. 3. Simulated results for 5 dosing schemes (*NT, S-I, S-II, S-III, S-IV*, see Table II), all with 500 mg total dose over a 10-week period. *S-I* through *S-IV* show significant improvement in tumor growth management compared to no treatment (NT). *S-III* and *S-IV* show the best profile but no significant difference between the two. Overall, outcome at the end of the treatment period is better than a constant infusion.

As an internal validation, we varied the P-gp induction constant (*R*) while holding all other parameters constant. Figure 4 is the simulated result for changes to tumor growth dynamics with changes in *R*. As the model predicts, increasing *R* consistently produced poorer tumor growth outcome. The behavior of P-gp induction with accumulated level of DOX in the ICF is shown in Fig. 5 (only *S-I* scheme is shown). As expected, P-gp profile rises and falls more slowly than that of ICF taking approximately 12 h (five P-gp half-lives) to reach its new steady-state value. Overall, *S-III* and *S-IV* were the dosing schemes that produced the least P-gp induction and correspondingly the best PD outcomes (Table III and Fig. 6).

DISCUSSION

In this work, a previously published (8,9) three-compartment pharmacokinetic model for doxorubicin cellular

Table I. Parameter Values Used in Simulations

Parameter	Assigned value	Reference	Comment
k_{10}	0.065 $days^{-1}$	Harashima *et al.*[12]	Taken directly
k_{12}	0.12 $days^{-1}$	Dordal[8]	Taken directly
k_{23}	138.24 $days^{-1}$	Dordal[8]	Taken directly
k_{30}	0.10 $days^{-1}$	None	Arbitrary estimation
V_{max}/K_m	3/1	Wielinga *et al.*[11]	Taken directly
R_0	0.10 $days^{-1}$	Maitra *et al.*[3]	Estimated from data
R	0.130 $days^{-1}$	Maitra *et al.*[3]	Estimated from data
k_{Pgp}	0.30 $days^{-1}$	Maitra *et al.*[3]	Estimated from data
α	0.125 $days^{-1}$	Jackson[9]	Taken directly
β	0.165 $days^{-1}$	Jackson[9]	Taken directly
δ	4.1×10^{-4} M	Jackson[9]	Taken directly
ε	1×10^{6} mg^{-1}	None	Fixed constant
λ	1 (P-gp unit)$^{-1}$	None	Fixed constant
n	1	None	Fixed constant

Table II. Dosing Schemes Used in Simulations

Dosing scheme	Schedule	Total dose	Total dose period
NT	No treatment	—	—
S-I	Constant infusion	500 mg	10 weeks
S-II[a]	50 mg IVB (IV bolus) QW (every week)	500 mg	10 weeks
S-III	200 mg IVB week 1, 33.3 mg IVB QW weeks 2–10	500 mg	10 weeks
S-IV	100 mg IVB week 1, 100 mg IVB week 2, 37.5 mg IVB QW weeks 3–10	500 mg	10 weeks

[a] *S-II* most closely resembles the actual recommended clinical dose.

transport was coupled to P-gp induction dynamics modulated by intracellular doxorubicin concentrations and to a pharmacodynamic model for tumor cell-kill. Key kinetic elements in the presented model are 1) dose-sensitive P-gp induction dynamics, 2) a required accumulated amount of A_{NUC} to trigger cell death, and 3) two different cytosolic exposure variables, *Pgp* and A_{NUC}, controlling P-gp induction and tumor cell death dynamics, respectively.

As an acquired resistance, overexpression of MDR genes encoding for P-gp has been qualitatively linked to intracellular DOX concentrations as well as other cytotoxic agents that are substrates for P-gp. Therefore, using A_{ICF} to modulate P-gp is more reasonable than using A_{ECF}. Additionally, A_{ICF} directly links the level of P-gp induction to the dosing profile applied, and it can partially account for time-lag differences due to ECF/ICF membrane permeation. Obviously, an empirical model as such does not account for the true mechanistic nature of protein induction and, therefore, does not assume a pre- or post-translational mechanism for induction. Rather than adding more complexity to the model, we chose to describe the "amount" or "level" of P-gp induction with a single state variable, *Pgp*.

Similar to the induction variable, *Pgp*, A_{NUC} is also a state variable directly linked to A_{ICF}. A_{NUC} is an inverse measure of the cells' overall viability, not just amount of DOX in the nucleus. In addition, A_{NUC} is also a state variable that encompasses the complex kinetics describing the pharmacological mechanisms of DOX, the required threshold of DOX exposure before cell death can occur, and DOX transport kinetics from the cytosol to its site of action.

To demonstrate the effect of modulation in P-gp induction on pharmacodynamic outcome, the induction rate constant (R) was varied while maintaining all other parameters constant (Fig. 4). Doubling or reducing R by half significantly altered the pharmacodynamic profile for tumor growth. Increasing R was consistent with poorer tumor growth outcome. whereas decreasing R was consistent with better tumor growth outcome. This result served, in part, as an internal validation as well as supported the view that a higher induced state of P-gp led to a lower intracellular DOX concentration, thereby lowering the extent of cell kill.

In the simulations, we attempted to modulate the P-gp level by applying different dosing schemes while maintaining an arbitrary 500 mg total dose over 10 weeks constraint. This constraint was applied with the consideration that, in reality, DOX has a limited total lifetime dose of about 450–500 mg/m^2 due to severe cardiotoxicity. As the simulation results show, our model predicted that fluctuations in P-gp level of the cancer cells due to the dosing scheme would influence the PD outcome. (Fig. 3, Table III). One might expect that a constant infusion (*S-I*), which provides constant exposure of drug to the cancer cell population at steady state, would produce the best pharmacodynamic outcome. Our model shows that the QW (every week) regimens (*S-II, III, and IV*) fare better in controlling tumor growth compared to the constant infusion. As shown in Table III, the QW treatments resulted in lower level of P-gp induction based on AUC value.

Although creating dosing regimens that lead to minimized P-gp induction is a sound initial step toward clinically relevant dosing optimization, more clinically useful optimizations would have to simultaneously minimize P-gp induction and minimize DOX's cardiotoxicity to maximize therapy.

Table III. Area Under the Curve (AUC) as Calculated from the Plots in Fig. 7 and Fig. 9.[a]

	AUC during treatment period	
Dosing scheme	Number of surviving cells	P-gp induction
NT	1.73×10^9	120
S-I	6.33×10^5	1408
S-II	4.86×10^5	1371
S-III	$\mathbf{3.98 \times 10^5}$	**1299**
S-IV	4.01×10^5	1342

[a] As shown, dosing scheme *S-III* produced the best PD and lowest extent of P-gp induction.

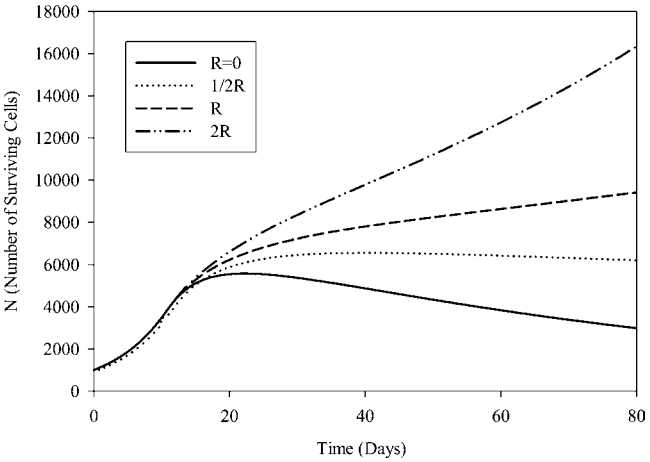

Fig. 4. Effects of varying the P-gp induction term (R) on tumor growth profile for a 500-mg doxorubicin constant infusion over 10 weeks (*S-II*). Solid line is the R value used in simulation. Increasing R, which corresponds to a more rapid increase in P-gp induction, produces a poorer tumor growth profile.

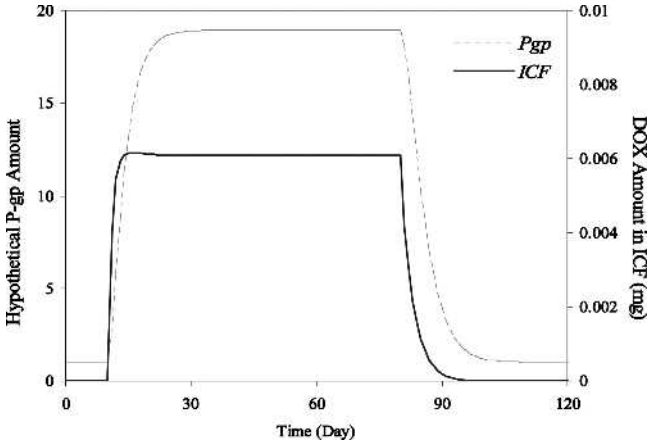

Fig. 5. A simulated result demonstrating the behavior of P-gp induction with accumulated level of DOX in the ICF after a 500 mg constant infusion of DOX over 10 weeks (*S-I*, see Table II).

The need for using the time-course of DOX's cardiotoxicity as a constraint, rather than a simple 500-mg total dose constraint, is quite clear from the clinical literature (13,14). For example, it has been clinically established that a constant infusion over 10 weeks (same as our *S-I* simulation) would lead to the least amount of cardiotoxicity (14). Yet, our simulation, based on minimizing P-gp induction, predicted that *S-I* would have the worst PD outcome. The clinical trade-off for reduced undesired effects may warrant a dosing regimen that does not fully minimize P-gp induction. The mechanism of cardiotoxicity appears to be mediated by doxorubicin-induced free radical release with subsequent apoptosis (15). The simple 500-mg total dose constraint allows for large front-loaded doses that might not be allowed under a toxicokinetic constraint that places an upper limit on DOX-induced free-radical exposure. This same kinetic constraint could easily be adapted to include other combination therapies, for example, paclitaxel (16), that decrease DOX exposure through the depletion of a shared co-factor or metabolic pathway.

In this work, we were limited to using literature data and parameters previously estimated from experimental data. The first steps in future modification of this model would involve rigorous model validation. Another model that has experimental merit (17) would be the inclusion of k_{32} to make the NUC compartment exchangeable. Crivellato *et al.* (17) have found in normal, LLC-PK_1 cells that DOX can enter the nucleus within 10 min, and it dissipates in approximately 2 h when viewed by fluorescence microscopy. Another consideration is to incorporate actual physiologic kinetic parameters so that dosing optimization would reflect true kinetics of DOX in patients, although a physiologic model may not capture the mechanistic essence presented in this cellular transport model. If available, data on tumor regression during therapy could very well be used to further validate this model. Additionally, future work should include toxicity constraints, such as maximum clinical input rate, concomitant therapies that reduce or increase toxicity, and toxicokinetic exposure.

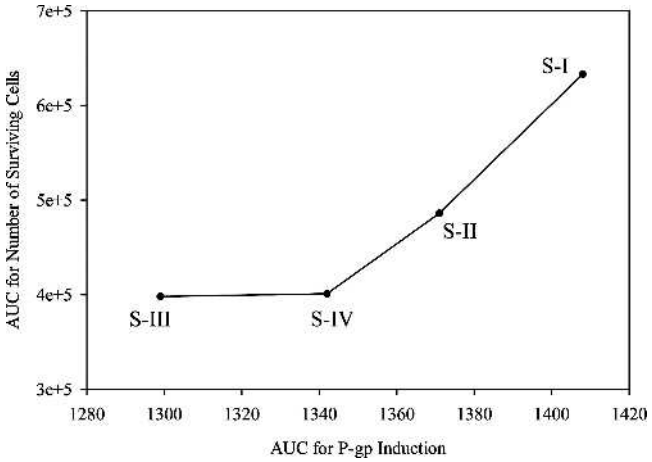

Fig. 6. Graphical display of Table III. Lower P-gp induction corresponds to better pharmacodynamic (PD) outcome (lower number of surviving cancer cells). S-I dosing scheme produces the higher P-gp induction and poorer PD outcome.

CONCLUSIONS

In summary, this paper presents a theoretical pharmacokinetic-pharmacodynamic model for predicting tumor growth outcome in the presence of doxorubicin-modulated P-gp induction. The pharmacokinetic component was based on estimated pharmacokinetic parameters of a cellular transport model. The presented model used two state variables, *Pgp* and A_{NUC}, which were directly linked to the dose through A_{ICF}, to determine the extent and time course of P-gp induction and cell kill, respectively. Future work should also include clinical toxicity constraints to improve optimal dosing schemes.

ACKNOWLEDGMENTS

This work was supported in part by the National Science Foundation GK-12 Grant award DGE0231796. Grant support from the Pacific Pharmacy Alumni Association is also greatly appreciated and acknowledged.

REFERENCES

1. C. Marbeuf-Gueye, M. Salerno, P. Quidu, and A. Garnier-Suillerot. Inhibition of the P-glycoprotein- and multidrug resistance protein-mediated efflux of anthracyclines and calceinacetoxymethyl ester by PAK-104P. *Eur. J. Pharmacol.* **391**:207–216 (2000).
2. J. Meesungnoen, J. P. Jay-Gerin, and S. Mankhetkorn. Relation between MDR1 mRNA levels, resistance factor, and the efficiency of P-glycoprotein-mediated efflux of pirarubicin in multidrug-resistant K562 sublines. *Can. J. Physiol. Pharmacol.* **80**: 1054–1063 (2002).
3. R. Maitra, P. A. Halpin, K. H. Karlson, R. L. Page, D. Y. Paik, M. O. Leavitt, B. D. Moyer, B. A. Stanton, and J. W. Hamilton. Differential effects of mitomycin C and doxorubicin on P-glycoprotein expression. *Biochem. J.* **355**:617–624 (2001).
4. M. Demeule, M. Brossard, and R. Beliveau. Cisplatin induces renal expression of P-glycoprotein and canalicular multispecific organic anion transporter. *Am. J. Physiol.* **277**:F832–F840 (1999).
5. X. Bian, T. D. Giordano, J. J. Lin, G. Solomon, V. P. Castle, and A. W. Opipari. Chemotherapy-induced apoptosis of S-type neuroblastoma cells requires caspase-9 and is augmented by CD95/Fas stimulation. *J. Biol. Chem.* **279**:4663–4669 (2004).
6. L. Lothstein, M. Israel, and T. W. Sweatman. Anthracycline drug targeting: cytoplasmic versus nuclear—a fork in the road. *Drug Resist. Update* **4**:169–177 (2001).
7. S. Fulda, H. Sieverts, C. Friesen, I. Herr, and K. M. Debatin. The CD95 (APO-1/Fas) system mediates drug-induced apoptosis in neuroblastoma cells. *Cancer Res.* **57**:3823–3829 (1997).

8. M. S. Dordal, A. C. Ho, S. M. Jackson, Y. F. Fu, C. L. Goolsby, and J. N. Winter. Flow cytometric assessment of the cellular pharmacokinetics of fluorescent drugs. *Cytometry* **20**:307–314 (1995).
9. T. L. Jackson. Intracellular accumulation and mechanism of action of doxorubicin in a spatio-temporal tumor model. *J. Theor. Biol.* **220**:201–213 (2003).
10. W. L. Jusko. A pharmacodynamic Model for cell-cycle-cpecific chemotherapeutic agents. *J. Pharmacokinet. Biopharm.* **1**:175–199 (1973).
11. P. R. Wielinga, H. V. Westerhoff, and J. Lankelma. The relative importance of passive and P-glycoprotein mediated anthracycline efflux from multidrug-resistant cells. *Eur. J. Biochem.* **267**:649–657 (2000).
12. H. Harashima, S. Iida, Y. Urakami, M. Tsuchihashi, and H. Kiwada. Optimization of antitumor effect of liposomally encapsulated doxorubicin based on simulations by pharmacokinetic/pharmacodynamic modeling. *J. Control. Rel.* **61**:93–106 (1999).
13. E. S. Lipshultz. Female sex and higher drug dose as risk factors for cardiotoxic effects of doxorubicin therapy for childhood cancer. *N. Engl. J. Med.* **26**:332 (1995).
14. B. Orthan. Doxorubicin cardiotoxicity: growing importance. *J. Clin. Oncol.* **17**:2294–2296 (1999).
15. P. Spallarossa, S. Garibaldi, P. Altieri, V. Manca, S. Nasti, P. Rossettin, G. Ghigliotti, A. Ballestrero, F. Patrone, A. Barsotti, and C. Brunelli. Carvedilol prevents doxorubicin-induced free radical release and apoptosis in cardiomyocytes in vitro. *J. Mol. Cell. Cardiol.* **37**:837–846 (2004).
16. E. A. Perez. Paclitaxel and cardiotoxicity. *J. Clin. Oncol.* **16**:3481–3482 (1998).
17. E. Crivellato, L. Candussio, A. M. Rosati, G. Decorti, F. B. Klugmann, and F. Mallardi. Kinetics of doxorubicin handling in the LLC-PK1 kidney epithelial cell line is mediated by both vesicle formation and P-glycoprotein drug transport. *Histochem. J.* **31**:635–643 (1999).